The structural basis of TRIM25-mediated regulation of RIG-I

Received for publication, November 28, 2024, and in revised form, February 4, 2025 Published, Papers in Press, February 28, 2025,
https://doi.org/10.1016/j.jbc.2025.108367

Yunlong Li[1,2,‡], Siqi Wu[1,2,‡], Xuyang Tian[3], Chen Kong[1,2], Wenbin Hong[1,2], Tianyichen Xiao[1,2], Songqing Wang[1,2], Zhiming Wei[1,2], Zhiming Su[1,2], Haixia Ren[1,2], Yunlong Song[1,2], Lichen Hu[1,2], Donghai Lin[4], Hongwei Yao[5], Jiahuai Han[1,2], Xueqin Chen[6,*], and Tianwei Lin[1,2,*]

From the [1]State Key Laboratory of Cellular Stress Biology, Innovation Center for Cell Signaling Network, State-province Joint Engineering Laboratory of Targeted Drugs from Natural Products, School of Life Sciences, Xiamen University, Xiamen, Fujian, China; [2]Cancer Research Center of Xiamen University, Xiamen, Fujian, China; [3]State Key Laboratory of Membrane Biology, Beijing Advanced Innovation Center for Structural Biology, Beijing Frontier Research Center for Biological Structure, School of Life Sciences, Tsinghua University, Beijing, China; [4]College of Chemistry and Chemical Engineering, Xiamen University, Xiamen, Fujian Province, China; [5]Institute of Molecular Enzymology, Soochow University, Soochow, Jiangsu, China; [6]Xiamen Key Laboratory of Clinical Efficacy and Evidence Studies of Traditional Chinese Medicine, The First Affiliated Hospital of Xiamen University, School of Medicine, Xiamen University, Xiamen, China

Reviewed by members of the JBC Editorial Board. Edited by Karen Fleming

TRIM25, an E3 ligase, is an important regulator to modulate the functions of retinoic acid inducible gene-I (RIG-I) and other factors in innate immunity. Herein the structural interaction between the 2CARD domain of RIG-I and the PRYSPRY domain of TRIM25 was investigated by NMR, X-ray crystallography, computer-assisted modeling, and cell-based assays to elucidate the complex structure of PRYSPRY/2CARD. The interacting model indicated that docking of 2CARD onto PRYSPRY brought two RIG-I molecules into a close proximity to form a dimer. The attachment of a short ubiquitin chain covalently by the TRIM25's E3 ligase activity was favorable for tethering a neighboring RIG-I dimer to form the tetrameric RIG-I by noncovalent interactions. The data supported the notion that the TRIM25–RIG-I interaction was important to activate the RIG-I pathway to suppress the replication of RNA viruses, such as vesicular stomatitis virus. This work provides a structural rationale to delineate the underlying mechanism of TRIM25 regulation of RIG-I.

Retinoic acid inducible gene-I (RIG-I) belongs to the RLR family responsible for sensing RNA cytoplasmic molecular patterns either from exogenous pathogens or endogenous damages (1, 2). It is comprised of two N-terminal caspase activation and recruitment domains (2CARD), a DECH-box helicase domain, and a C-terminal regulatory domain that recognizes characteristic dsRNA or ssRNA (3–5). RIG-I is initially in an autoinhibited state with its 2CARD domain associating with the helicase domain (4, 6, 7). The binding of RNA and ATP changes the RIG-I conformation from an autoinhibited state to an activated state with the release of 2CARD (8). The release of 2CARD results in the formation of oligomers first and then filaments with the downstream MAVS (9, 10). This activation process is regulated by E3 ligases (11, 12).

TRIM25 is an E3 ligase which was first reported to be responsible for activating RIG-I signaling (13, 14). TRIM25 is comprised of a really interesting new gene (RING) domain, two B-box domains, a coiled-coil domain, and the C-terminal PRYSPRY domain (PSpry) (15). The RING domain is a self-associating and zinc-binding motif responsible for the TRIM25's E3 ubiquitin ligase activity and for the interaction with E2 ubiquitin conjugating enzyme (16–18). Most RING domains in the TRIM family function as transient dimers upon ligand binding (19). The self-association of TRIM25 is mainly mediated by the coiled-coil domain, and the dimerization or higher order oligomerization was shown to be necessary for the catalytic activity (16, 20). Two coiled-coil domains form a 170 Å antiparallel dimer, which positions the two RING domains at the opposite ends of the dimer (21). The C-terminal PSpry is responsible for the direct interaction with 2CARD (15).

Despite many data supported the notion that TRIM25 was important for regulating RIG-I, its role in the RIG-I activation was questioned (22–24). It was shown that another E3 ubiquitin ligase RIPLET (RNF135), not TRIM25, was sufficient to ubiquitinate and activate RIG-I, and TRIM25 could be dispensable for activating RIG-I in cells with low TRIM25 activity. Nevertheless TRIM25's role in regulating RIG-I was still evident with the finding of multiple proteins or RNAs that could suppress the innate immunity by hindering the TRIM25–RIG-I interaction and the subsequent ubiquitination of RIG-I to restrict virus replications (25–36). There were many data and models to conciliate TRIM25's role in regulating RIG-I, such as the "sequential ubiquitination" model that might reconcile the roles of TRIM25 and REPLET (37) among others, but data are still needed to support TRIM25's role in regulating RIG-I. In this report, the complex structure between interacting domains from RIG-I and TRIM25 was determined by a combination of NMR, X-ray crystallography,

‡ These authors contributed equally to this work.
* For correspondence: Tianwei Lin, twlin@xmu.edu.cn; Xueqin Chen, xqchen@xmu.edu.cn.

computer-assisted modeling, and cell-based assays. Mutations at the interface between the two proteins in the complex structure could perturb the interaction between TRIM25 and RIG-I and hampered the activation of RIG-I pathway, supporting the notion that TRIM25 is an important E3 ligase to regulate the functions of RIG-I. Docking of RIG-I onto the TRIM25 structure suggested that both covalent and noncovalent interactions with the ubiquitin chains were important for the formation of the tetrameric RIG-I structure to activate the antiviral pathway. This work provides a structural framework for further understanding the TRIM25's role in regulating the RIG-I pathway.

Results and Discussion

Identifying TRIM25 residues in direct interaction with RIG-I

To unravel the structural basis of interaction between TRIM25 and RIG-I, the interacting domains from the two proteins, PSpry of human TRIM25 and 2CARD of human RIG-I, were produced. However, the recombinant PSpry and 2CARD could not form a stable complex and the cocrystallization of these two proteins only led to the structure determination of PSpry by X-ray crystallography (Fig. S1, Table S1, PDB: 9IUN).

To circumvent the difficulty of solving the complex structure, chemical shift perturbation by NMR was employed to investigate the interaction between the two proteins (38). The resonance assignments covering 95% of the residues of PSpry's backbone amides were previously reported (39). In ^{1}H,^{15}N-HSQC titration experiments, peak position and intensity changes in the HSQC spectra of ^{15}N-labeled PSpry with the addition of unlabeled 2CARD implicated several PSpry residues either directly participating in the interaction with 2CARD or involving in structural changes due to the interactions between PSpry and 2CARD. The ratio of 1:1 between ^{15}N-labeled PSpry and unlabeled 2CARD in 0.2 mM were used for the data acquisition after experiments with different ratios of the two proteins. The peak intensity and peak position changes in the ^{1}H,^{15}N-HSQC spectrum of ^{15}N-labeled PSpry after the addition of unlabeled 2CARD were evident (Fig. 1*C*, Fig. S2*B*) and the associated PSpry residues could be identified with the resonance assignments (Fig. 1*A*). Four residues, Y463, S473, A479, and F618, were with significant peak intensity changes (line-broadening) and they were all on the north side (upper side as in a map) of the PSpry structure (Fig. 1*B*, Table S2). Peak position changes were also observed for residues A471, S473, A479, T496, G525, K573, A614, F618, T623, and I626 (Table S2), which were also distributed lopsidedly towards the north pole of the molecule (Fig. S2*A*). Residues Y463, S473, A479, and F618 were located at the flexible loops of PSpry on the surface. Those perturbed residues that were not on the surface or were insignificantly influenced by the chemical shift perturbations could be "passive" residues which were affected by the "active" residues in direct binding (40). Similar residues were also identified in the flexible loops of RIPLET PSpry in the RIPLET PSpry–RIG-I Δ2CARD complex (41).

A model of the PSpry/2CARD complex

An initial model of the PSpry/2CARD complex using the program Discovery Studio was made based on the residues identified in the chemical shift perturbation experiments. Initially three PSpry residues, A471, T496, and F618, were chosen as the restraint residues (Fig. 2*A*), as these residues were distributed on different spots on the putative binding surface. The calculation produced a single cluster of complex structures (Fig. 2*B*). For comparison, a model was also calculated without the restraints of those three residues (Fig. S2*C*). The orientation of 2CARD in the model without the restraints, although was with the similar general orientation and interface, was with a 2 degrees rotation from the restraint docking (Fig. S2*D*). The final model was refined with the ROSETTA suite (42). An attempt was also made to generate the model with AlphaFold2 and 3, but no output was compatible with the experimental data.

Formation of the complex was dominated by intermolecular interactions between residues located on the loops of PSpry and the β sheet surface of 2CARD, such as residues A466, K469, S480, E483, T496, Y497, C498, R541, A620 in PSpry and residues K45, N47, G49, K115, E138, K146, A150, E153, K154 in 2CARD (Fig. 2, *C* and *D*, Table S3). These residues buried a surface area of 1,226.6 Å^2. No major conformational adjustment was required for forming the complex between the crystal structures of PSpry and 2CARD as the r.m.s.d. for the overlapping Cα atoms of crystalline PSpry and the PSpry structure in the complex was 0.141 Å and the r.m.s.d. for the Cα atoms between the complexed 2CARD and free 2CARD in Protein Data Bank (PDB: 4NQK) was 0.460 Å.

PRE data corroborates the PSpry/2CARD complex structure

The acquisition of HSQC spectra for the chemical shift perturbations with ^{15}N-labeled 2CARD was not achievable as the protein precipitated at the concentrations required. To obtain the complementary data for 2CARD docking onto the PSpry structure, paramagnetic relaxation enhancement (PRE) was employed to obtain the experimental restraints on the interaction between 2CARD and PSpry by attaching specific paramagnetic spin label in 2CARD and detecting affected ^{15}N-labeled residues in PSpry for long-range distance restraints in HSQC experiments.

There were four Cys residues in 2CARD, C130, C136, C143, and C158. Among these, residues C130, C136, and C143 could be mutated to Ser residues. Hence, a unique thiol group from residue C158 was used for the site-specific spin labeling. The distance from the thiol of C158 to the nearest residue in PSpry was 6.5 Å in the interacting model. This thiol was deemed suitable for the PRE experiments since any signal from the ^{15}N-labeled PSpry residues could be influenced by the NOE as long as they were about 20 Å or less from the spin label in 2CARD (43). A spin label containing a stable nitroxyl radical, (1-oxyl-2,2,5,5-tetramethyl-3-pyrroline-3-methyl) methane thiosulfonate (MTSL), was attached to the thiol of C158 in 2CARD (Fig. S3*A*) (44). A series of PSpry residues whose signals were perturbed by the spin label were obtained by examining the ^{1}H,^{15}N-HSQC spectra of PSpry with or without

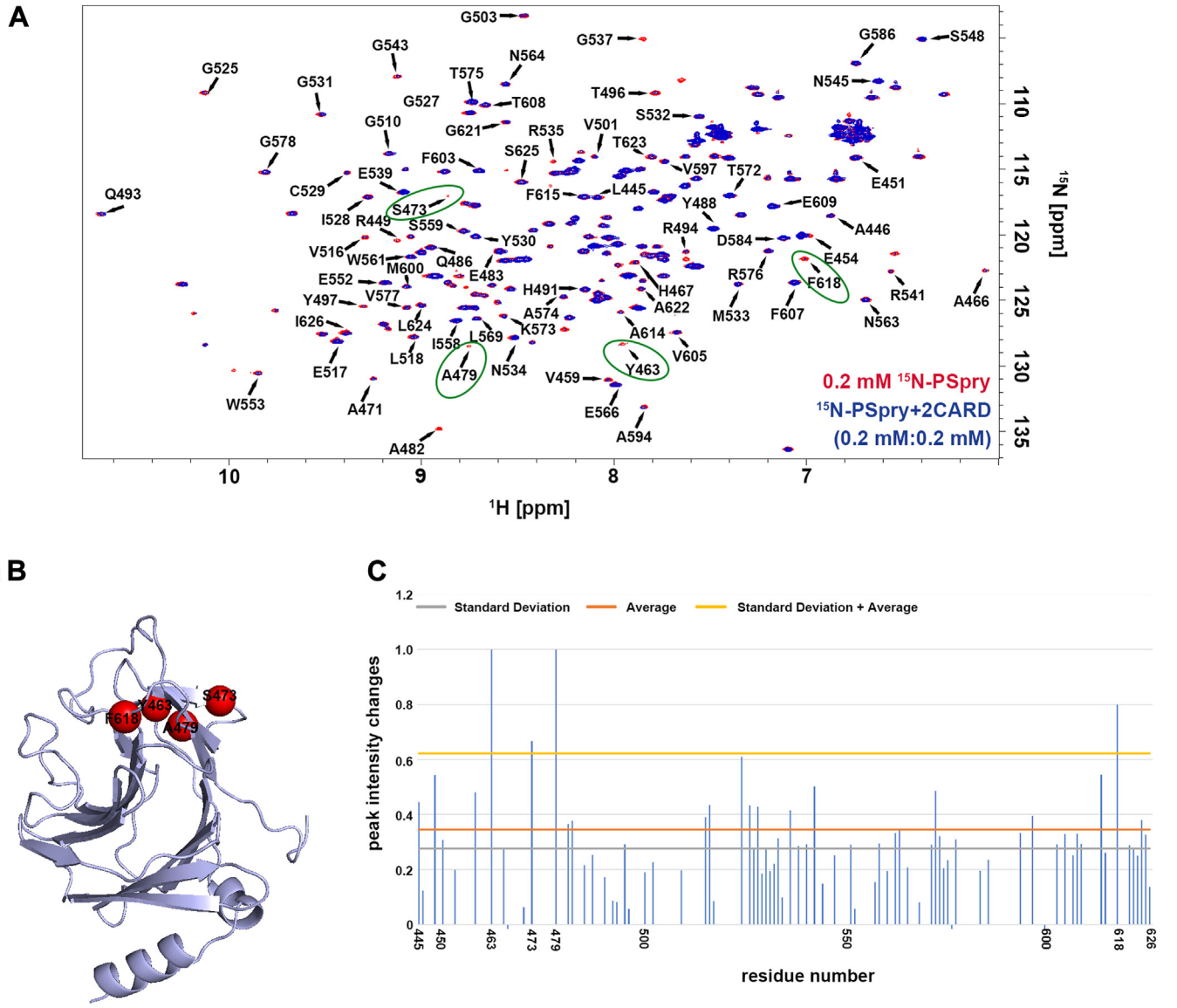

Figure 1. Identifying PSpry residues in direct interaction with 2CARD. *A*, overlay of the ^{1}H,^{15}N-HSQC spectra of ^{15}N-labeled PSpry (*red*) and the mixture of ^{15}N-labeled PSpry and unlabeled 2CARD (*blue*). The peaks with line-broadening were indicated with *circles*. *B*, residues with significant line-broadening in the spectrum were indicated by *spheres* in the structure of PSpry. *C*, analysis of the peak intensity changes in the ^{1}H,^{15}N-HSQC spectrum of ^{15}N-labeled PSpry with the addition of unlabeled 2CARD in a molar ratio of 1:1.

the MTSL-labeled 2CARD (Fig. 3*A*, Fig. S3, *B* and *C*). The PSpry residues with peak intensity and position changes in the PRE experiments were consistent with the interacting model based on the restraints by chemical shift perturbations in the HSQC spectra of ^{15}N-labeled PSpry, with the identification of additional residues on the interacting surface, such as Y497, in PSpry (Table S2). The PSpry residues influenced by the spin label in 2CARD clustered around the interacting interface and spread southward with reduced perturbing strength (Fig. 3, *B* and *C*, Fig. S3*D*).

Mutations on the binding surface impairs the interaction between TRIM25 and RIG-I

The interacting model of the PSpry–2CARD complex was further analyzed by the cell-based approach. A series of mutations on the contact interfaces between the two proteins were generated for Co-immunoprecipitation (Co-IP) experiments (Fig. S4*A*). Single mutations of PSpry^{A471W}, PSpry^{S480W}, PSpry^{E483A}, PSpry^{T496G}, and PSpry^{Y497A} in the contact surface could be generated, which dampened the interaction between PSpry and 2CARD. Mutations of PSpry^{Y463A}, PSpry^{R489G}, and PSpry^{W616A} were also made but they interfered little with the interaction in Co-IP experiments as they were not in the interacting interface (Fig. 4*A*, Fig. S4*A*).

Mutations of 2CARD^{A150W}, 2CARD^{G49W}, 2CARD^{N47W}, 2CARD$^{K45W/N47W/G49W}$, and 2CARD$^{E138W/K146W/A150W/E153W/K154W}$ could also be made on the interface with PSpry (Fig. S4*A*). All of these mutations impaired the interactions between PSpry and 2CARD (Fig. 4*B*).

Influence of the above mutations on the signaling activity of RIG-I in 293T cells was also examined. WT 2CARD and PSpry

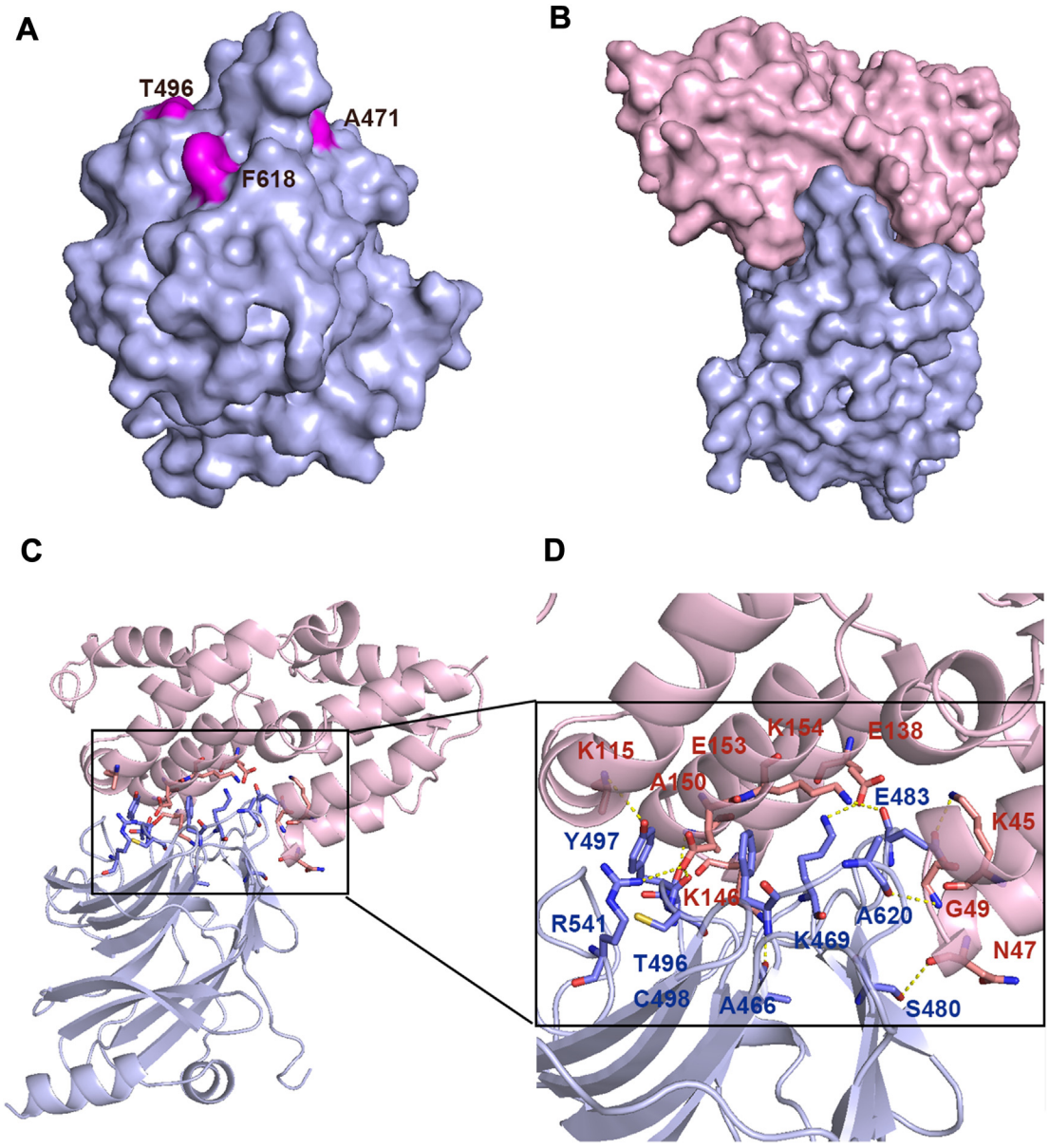

Figure 2. NMR-based model of PSpry/2CARD complex. *A*, three residues were chosen as the restraints for modeling, which were shown in *magenta*. *B*, the complex model of PSpry (*light blue*) and 2CARD (*light pink*) with restraint using the data from the experiments of chemical shift perturbation. *C*, the complex structure of PSpry and 2CARD in ribbon diagram. *D*, close-up view of the interface between PSpry and 2CARD. The interacting residues were shown as ball-and-stick.

transfected together potently induced the IFN-β and NF-*k*B promoter activity, as was reported previously (14). Mutations on the interface residues in 2CARD such as 2CARD^{A150W}, 2CARD^{G49W}, and 2CARD^{N47W}, as well as the triple mutation of 2CARD$^{G49W/N47W/K45W}$, quintuple mutation of 2CARD$^{E138W/K146W/A150W/E153W/K154W}$, showed markedly reduced IFN-β and NF-*k*B promoter activation, while those mutations that were not on the interface, such as 2CARD^{E44A} served as a negative control in this case, exerted no influence on the IFN-β promoter activation (Fig. 4*C*). Mutants of PSpry such as PSpry^{E483A} and PSpry^{Y497A} showed markedly reduced IFN-β and NF-*k*B promoter activation. While PSpry^{Y463A}, PSpry^{R489G}, or PSpry^{W616A} influenced the IFN-β and NF-*k*B expressions, they were of negligible influence on the interaction in Co-IP experiments. Residues Y463, R489, and W616 were close to, but not on, the interacting interface, so it might not be a surprise that their mutations did not have a significant impact on the Co-IP experiments. It was previously reported that PSpry^{Y463A} and PSpry^{R489G} could affect the activity but maintaining the interaction (45). In contrast, PSpry^{A471W} and PSpry^{F618A} induced IFN-β and NF-*k*B promoter activity in the similar manner as WT PSpry (Fig. 4*D*). Although PSpry^{A471W}, a mutation with a bulky residue, interfered in the interaction between PSpry and 2CARD in Co-IP experiments, the

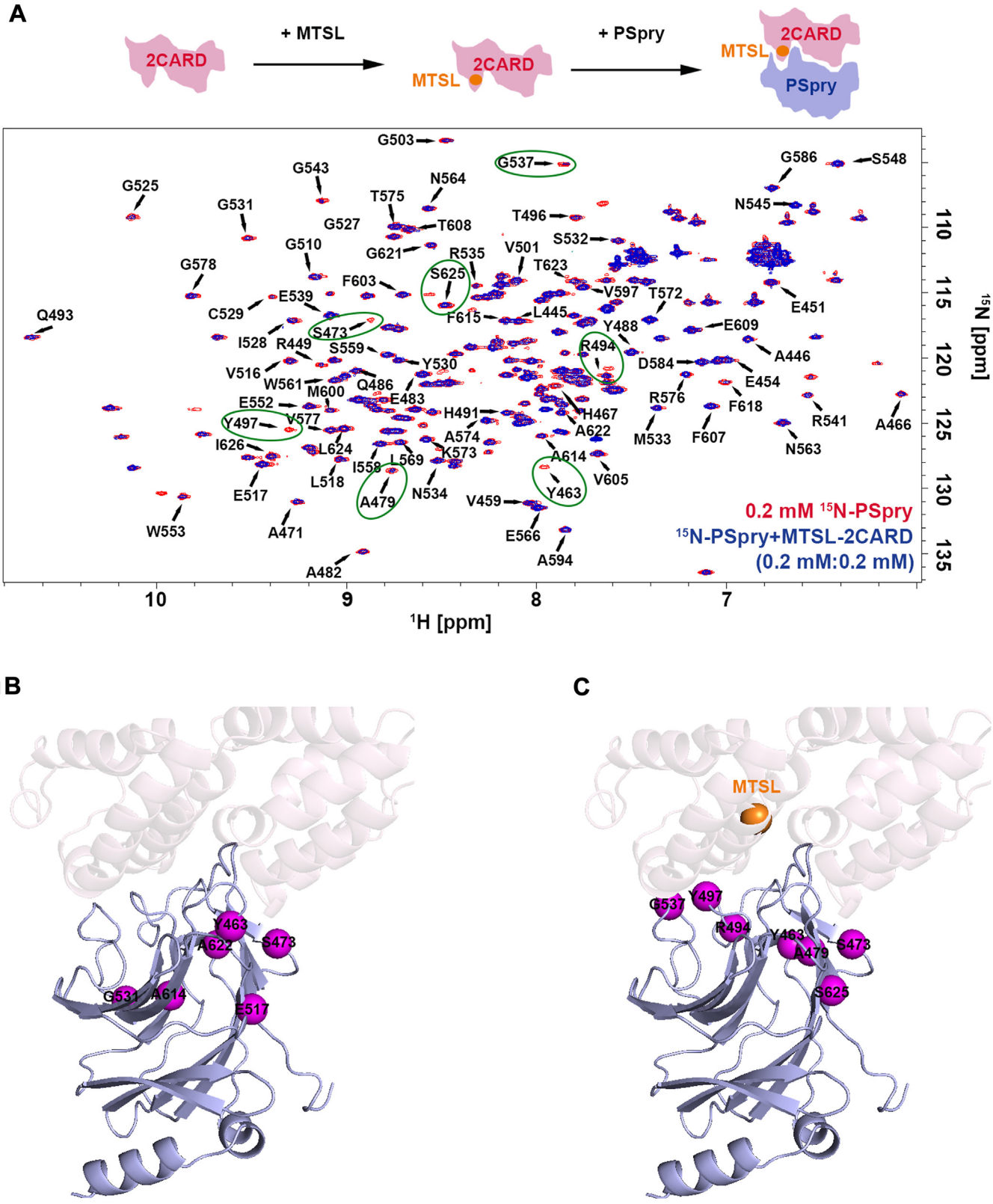

Figure 3. PRE experiments supporting the docking model of PSpry/2CARD. *A*, *top*: schematic illustration of the labeling of MTSL for the PRE experiments; *bottom*: overlay of the ^{1}H,^{15}N-HSQC spectra of ^{15}N-labeled Pspry (*red*) and of the mixture of ^{15}N-labeled PSpry/2CARD/MTSL (*blue*). Residues with peak intensity changes were indicated with *circles*. B, identification of interacting PSpry residues by the ^{15}N-labeled Pspry and 2CARD without the MTSL spin label. Protons in the backbone amide with significant peak intensity change were mapped onto the model of PSpry/2CARD. *C*, identification of interacting PSpry residues by the ^{15}N-labeled Pspry and 2CARD attached with the MTSL spin labels. Protons in the backbone amide with significant peak intensity change were mapped onto the model of PSpry/2CARD.

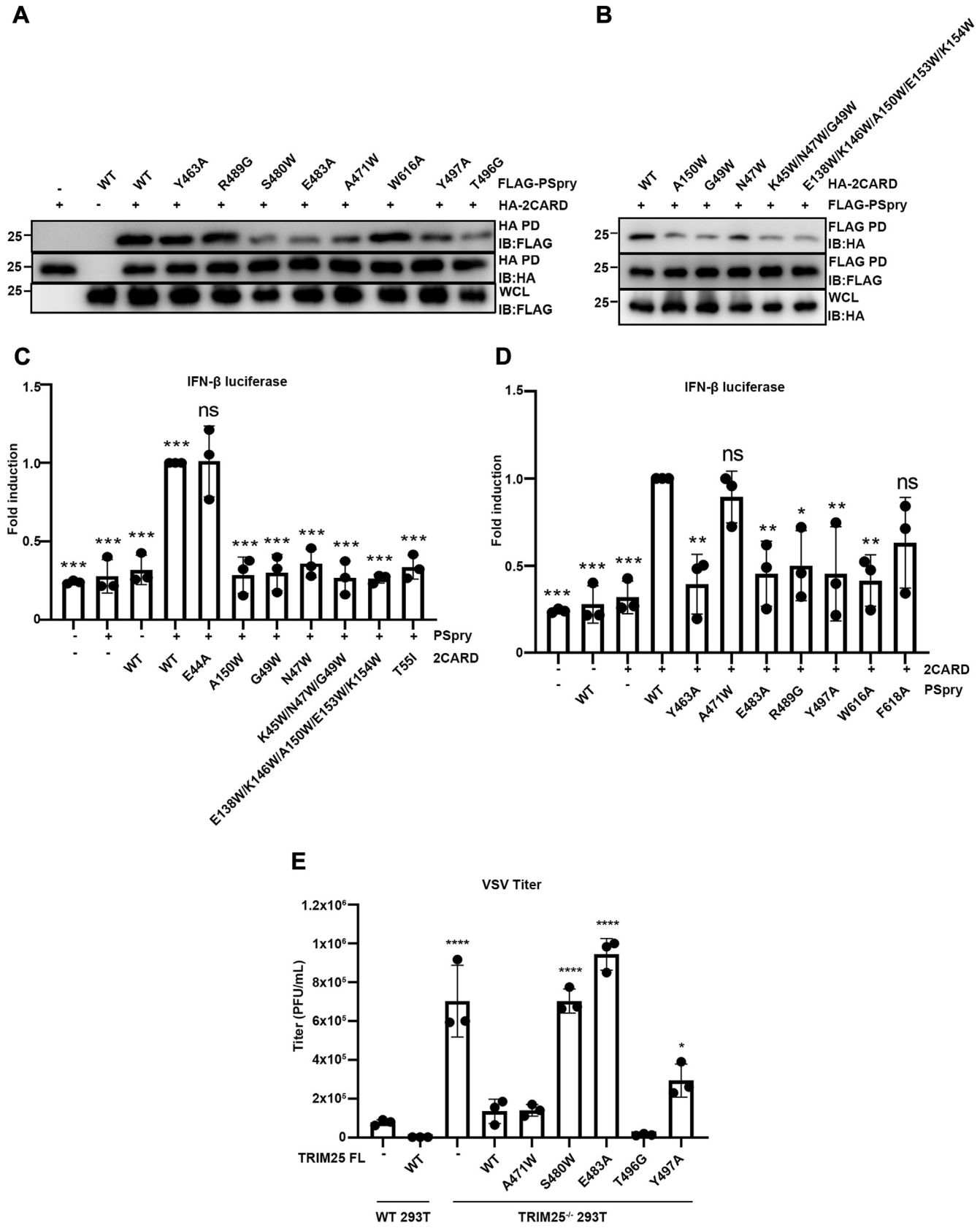

Figure 4. Mutations on binding surface of PSpry/2CARD model impaired the TRIM25 regulation of RIG-I. *A*, mutations on the PSpry-interacting surface with 2CARD. HEK293T cells transfected with FLAG-PSpry or the indicated mutants with the vector or HA-RIG-I 2CARD were used for the HA pull down. Whole cell lysates were subjected to IP with anti-HA beads and immunoblotting with α-FLAG antibodies. *B*, effect of 2CARD mutations on its interaction with PSpry. HEK293T cells transfected with HA-2CARD or the indicated mutants with vector or FLAG-PSpry were used for the FLAG pull down. Whole cell lysates were subjected to IP with anti-FLAG beads and immunoblotting with α-HA antibodies. *C*, effect of 2CARD mutants on the signaling activity of RIG-I, as measured

remaining interaction was still enough to induce the IFN-β and NF-*k*B promoter activity, as the mutation, albeit weakened, did not abolish the interaction (Fig. 4*A*). A TRIM25-knockout (TRIM25$^{-/-}$) in HEK 293T cells was also generated for reconstituting the TRIM25 activity with the transfection of either FLAG-tagged WT TRIM25, TRIM25^{A471W}, TRIM25^{S480W}, TRIM25^{E483A}, TRIM25^{T496G}, or TRIM25^{Y497A} to assess the influence on the replication of vesicular stomatitis virus (VSV) (Fig. S4*B*). There was an about 9-fold increase in the virus replication in TRIM25$^{-/-}$ cells after 48 h as compared to that in WT 293T cells. This increase in virus replication was suppressed after TRIM25 was introduced into the TRIM25$^{-/-}$ cells, as was previously showed (Fig. 4*E*, Fig. S4*C*) (34–36, 46). When the native sequence of TRIM25 was replaced by a single mutation of either S480W or E483A, the virus replicated in a manner as there was no WT TRIM25. The introduction of TRIM25^{Y497A} into the TRIM25$^{-/-}$ cells could partially suppress the virus replication, and the introduction of TRIM25^{T496G} also led to the decrease of viral titers significantly (Fig. 4*E*). Only TRIM25^{A471W} showed negligible influence on the virus replication, which was consistent with the Luciferase assays (Fig. 4, *D* and *E*). These data supported the NMR-based model for the complex structure between Pspry and 2CARD and arguing for the importance of TRIM25–RIG-I interaction for the RIG-I's antiviral activity.

A model for TRIM25 facilitating the activation of the RIG-I pathway

To make a model for the TRIM25–RIG-I interaction, the PSpry–2CARD complex structure determined here was superposed onto the PSpry structure in the oligomeric CC/PSpry structure (45), which resulted in no steric clash (Fig. 5*A*). The helicase/CTD domain structure of RIG-I (PDB entry 7JL3) was then added to the CC/PSpry/2CARD model (Fig. 5*B*). Two RIG-I molecules binding to the two neighboring PSpry in close proximity in the oligomeric TRIM25 were with an angle favorable for the formation of a RIG-I dimer with a twist. It was reported that the shortest polyubiquitin chain to form the tetrameric RIG-I was with three ubiquitin units (13). As distance of two RIG-I dimers on TRIM25 in our structure was within the length of three connecting ubiquitin units (Fig. 5*B*), it is possible that a polyubiquitin chain with at least three connecting ubiquitins covalently attached to a dimeric RIG-I could interact with the neighboring RIG-I dimer non-covalently to form the "lock-washer" tetrameric RIG-I to activate the signaling pathway (Fig. 5*C*) (47).

In summary, RIG-I is a key member of the RLR family regulated by E3 ligases for sensing RNA cytoplasmic molecular patterns either from exogenous pathogens or endogenous damages (13, 14). However, the role that TRIM25 played in regulating RIG-I was disputed with the find that another E3 ligase, RIPLET, was sufficient to ubiquitinate and activate RIG-I without the participation of TRIM25 (22–24). Yet, there are still abundant data supporting the role that TRIM25 plays to regulate the function of RIG-I (25–36). It is of great interest to unravel TRIM25's mechanism of regulating the functions of RIG-I. In this study, it was shown that TRIM25 could specifically interact with RIG-I to form a complex through their interacting domains. The determination of the complex structure between the interacting domains allowed mutations to be made at the interface, which attenuated RIG-I's antiviral activity. An interacting model was made between the full-length proteins of RIG-I and TRIM25, which favored the formation of a RIG-I dimer due to the close proximity of two RIG-I monomers. As the ubiquitin chain covalently attached to a RIG-I dimer by the E3 ligase activity of TRIM25 could interact with a neighboring RIG-I dimer through noncovalent interactions, it was plausible that the tetrameric RIG-I could be formed between two RIG-I dimers for activating the antiviral pathway. This work provides glimpse into the initial phase of forming the fibrous RIG-I/MAVS structure to activate an innate immune response and a structural framework for further understanding TRIM25's role to regulate the RIG-I pathway.

Experimental procedures

Protein expression and purification

The cDNA encoding the human PRYSPRY (PSpry) sequence (residues 433-630) in GenBank (accession number BC016924) and the human cDNAs for 2CARD (1-200) based on the sequence encoding RIG-I (GenBank accession number AF038963) were cloned by PCR. The constructs were made with the pET28a expression vectors with C-terminal His-tag for expression in *Escherichia coli* BL21 (DE3) cells. The molar extinction coefficient used for spectrophotometric protein concentration analysis for PSpry and its mutants was 44390 M^{-1} cm^{-1}. The yield for the PSpry production was 15 mg/ml. The molar extinction coefficient used for spectrophotometric protein concentration analysis for 2CARD and its mutants was 38180 M^{-1} cm^{-1}. The yield for the 2CARD production was 10 mg/ml.

PSpry and 2CARD expressions in *Escherichia coli* BL21 (DE3) cells were induced at A_{600}=0.6 by the addition of 0.2 mM IPTG and the cultures were allowed to grow for additional 16 h at 16 °C with shaking at 160 rpm. For the production of ^{15}N-labeled PSpry, the proteins were prepared by growing the bacteria in M9 medium containing $^{15}NH_4Cl$. The cells were harvested, centrifuged, resuspended in a lysis buffer (20 mM Tris–HCl, pH 7.6, 200 mM NaCl, 5 mM 2-mercaptoethanol), and lysed by sonication. The proteins were first purified by Ni-affinity chromatography with an elution buffer (25 mM Tris–HCl, pH7.6, 200 mM NaCl, 300 mM imidazole) and further purified by Superdex75 16/60

by the IFN-β promoter reporter assay. *D*, effect of PSpry mutants on the signaling activity of RIG-I, as measured by the IFN-β promoter reporter assay. *E*, virus replication of WT and TRIM25$^{-/-}$ 293T cells after transfected with the vector, WT TRIM25, or the indicated mutants. Cells were infected with 0.00000022 pfu per cell of Vesicular stomatitis virus. Error bars represent standard error from three independent experiments. Asterisks indicate significant t tests comparisons (*$p < 0.01$).

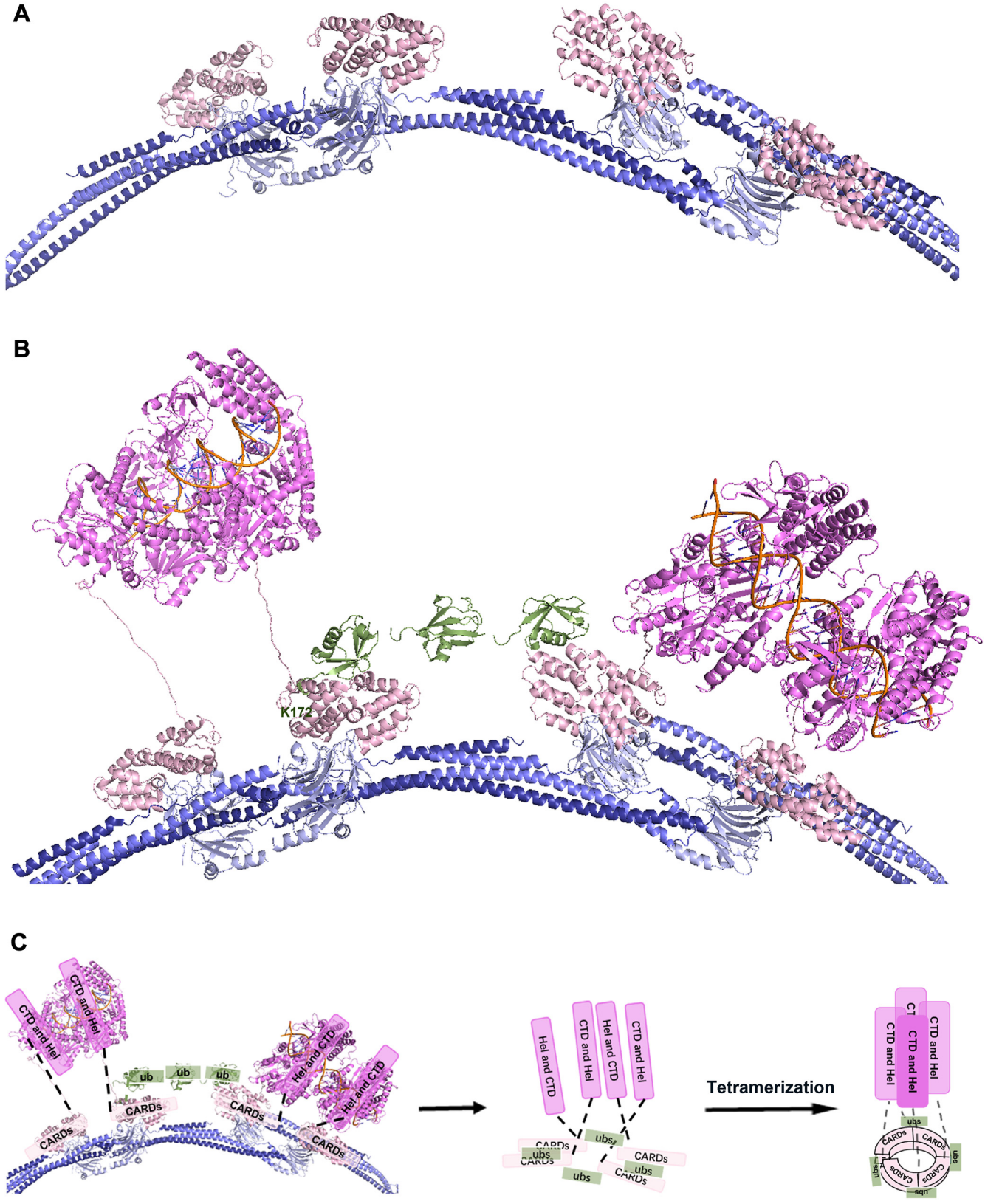

Figure 5. A model for TRIM25 and RIG-I interaction. *A*, modeling the CC/PSpry/2CARD complex by superposing the PSpry/2CARD structure (PSpry in *light blue*, 2CARD in *light pink*) onto the PSpry structure in the PSpry/CC complex structure (PDB code: 6FLN, CC in *dark* and *slate blue*). *B*, a RIG-I structure (PDB code: 7JL3) was added to the CC/PSpry/2CARD model (RIG-I: 2CARDs in *light pink*; helicase and CTD in *violet*; TRIM25: CC in *dark* and *slate blue*, PSpry in *light blue*; Ubiquitin chain in smudge, modeling from PDB entry 3HM3). A ubiquitin chain with three ubiquitin units attached to a dimer of RIG-I 2CARD was long enough to reach the neighboring 2CARD dimer with noncovalent interactions. *C*, a schematic illustration of TRIM25 interaction facilitating the tetramerization of the RIG-I.

(GE Healthcare) equilibrated with 20 mM Tris pH8.0, 10 mM NaCl, and 2 mM DTT for crystallization.

Crystallization, data collection, and structure determination

Purified PSpry was concentrated to 7 mg/ml and crystallized by hanging-drop vapor diffusion at 277 K with or without 2CARD. After screening by using Hampton crystal screening kits, the crystals were obtained by mixing 1.2 μl of the protein solution and 1 μl of the reservoir solution containing 100 mM Na citrate pH5.0 and 4 M NaCl in 4 °C. Crystals were transferred to a cryo-solution consisting of the reservoir solution supplemented with 23% glycerol, mounted in a nylon loop, and then flash-cooled in liquid nitrogen for data collection.

X-ray data collection, processing, and structure determination

The X-ray diffraction data were collected at Beamline BL17U1 in Shanghai Synchrotron Radiation Facility with an ADSC Quantum 315r CCD detector and processed with the HKL2000 package. The initial phases for the selenomethionine-labeled PSpry were obtained from a SAD experiment. Data were integrated and scaled with the HKL2000 package. The structure of PSpry was solved and refined with CCP4 (48), PHENIX (49), and COOT (50). Structural alignments and graphical representations were made with PyMOL.

HSQC titration of ^{15}N-labeled PSpry with unlabeled 2CARD

NMR data were acquired at 25 °C on an 850 MHz Bruker AVANCE III spectrometer. The 850 MHz spectrometer was equipped with a 5 mm TCI Cryoprobe. The backbone resonance assignments of PSpry were made previously (BMRB number 25267) (39). The ^{15}N-labeled PSpry was concentrated to 0.2 mM in 90% buffer with 10% D_2O for the ^{1}H-^{15}N HSQC experiments on a Bruker AVANCE III 850 MHz spectrometer at 298K. The protein was in a buffer containing 20 mM Tris (pH 7.3), 200 mM NaCl, 50 mM arginine, 50 mM glutamic acid, and 7 mM DTT. The formation of the PSpry/2CARD complex was confirmed by titration analysis with the addition of unlabeled 2CARD to the ^{15}N-labeled PSpry to mole ratios of 1:1 (the final concentration of ^{15}N-labeled PSpry was 0.2mM) for changes in peak position and peak intensity of the PSpry backbone amide resonances in ^{15}N/^{1}H HSQC experiments. All spectra were processed with NMRPipe/NMRDraw and analyzed using Sparky and Topspin. Ambiguous peak positions were not included in the analysis. Peak intensities and positions in NMR titrations were calculated with Sparky. Significantly perturbed resonances of PSpry were analyzed by using the equation: $\Delta\delta=[(\Delta\delta^{1}H)^2+(\chi^{*}\Delta\delta^{15}N)^2]^{1/2}$ (normalized for proton with the scale factor χ=0.13 established from estimates of atom-specific chemical shift ranges in a protein environment (51)). Significant peak intensity changes of PSpry were analyzed by using the equation: $1-I/I_o$, where I is the peak intensity in the presence of unlabeled 2CARD and I_o is the peak intensity in the absence of unlabeled 2CARD. The values higher than their A (Average)+SD (Standard Deviation) were selected and mapped onto the structure to identify the binding residues.

Mutagenesis and spin-labeling of 2CARD

2CARD constructs containing single cysteine residues were generated by mutating three of the four cysteine residues to serine (C130S, C136S, and C143S) leaving the lone C158 for spin labeling. All mutations were confirmed by DNA sequencing over the entire ORF. The mutant was modified with the thiol-specific spin-label reagent MTSL (Sigma). The 2CARD mutant at a concentration of 0.36 mM was mixed with MTSL at a ratio of 1:1 and incubated overnight at 4 °C in 20 mM Tris–HCl (pH 7.3), 100 mM NaCl, 50 mM arginine, 50 mM glutamic acid, and 7 mM TCEP. Unreacted spin labels were removed by dialysis at 4 °C overnight. Labeled and unlabeled 2CARD was added to the ^{15}N-labeled PSpry to a mole ratio of 1:1 (the final concentration of ^{15}N-labeled PSpry was 0.2mM) to obtain the HSQC spectra.

The interacting model for the PSpry and 2CARD complex

The crystal structure of PSpry determined in this work and 2CARD (PDB: 4NQK) were used for docking with the program ZDock in Discovery Studio (Accelrys Software Inc.). PSpry was the receptor and 2CARD was the ligand. Residues A471, T496, and F618 in PSpry were assigned as the key binding residues. Based on the RMSD for all atoms, the docking poses were clustered and ranked by scores. Poses from each cluster with high ZDock scores were selected and minimized by RDock using CHARM force field. One complex structure was identified at the top of ten binding poses ranked by E_RDock value, which also had the largest number of residues identified in the NMR experiments. This model was further optimized by interaction analysis and energy minimization. The complex structure was further refined with the ROSETTA suite (42). Structural alignments and graphical representations were generated with PyMOL.

Cell culture and transfection

HEK293T cells (ATCC) and Vero E6 cells (ATCC) were cultured in Dulbecco's modified Eagle's medium (Gibco) supplemented with 10% heat-inactivated fetal bovine serum (FBS, Gibco), 100 U/ml penicillin/ 100 μg/mL streptomycin at 5% CO_2 at 37 °C. hPSpry-FLAG and h2CARD-HA and relevant mutants were cloned in pBOB vectors and verified by sequencing. Cells were transfected using Lipofectamine 2000 (Invitrogen) according to manufacturer's instructions.

Co-immunoprecipitation and immunoblot analysis

PSpry-flag, 2CARD-HA, and their mutants were transfected into HEK293T cells. Cells were lysed in a lysis buffer (150 mM NaCl, 20 mM Tris–HCl, pH 7.5, 1% Triton X-100, 1 mM EDTA, 1 mM EGTA, 2.5 mM sodium pyrophosphate, and 1 mM β-glycerophosphate) with a protease inhibitor cocktail on ice for 1 h. The cell component was removed by centrifugation at 13,000 rpm for 15 min and the supernatant was mixed with anti-HA Magnetic Beads (Thermo Fisher

Scientific) on rotator at 4 °C for 1 h. The supernatant was removed and the magnetic beads were washed twice. SDS loading buffer was added to the beads and the sample was boiled for 10 min for electrophoresis.

For immunoblot analysis, proteins were resolved by SDS-PAGE and transferred onto PVDF membranes. The PVDF membranes were incubated with anti-HA (1:2000, Proteintech), anti-Flag (1:2000, Proteintech), or anti-TRIM25 (1:1000, Proteintech) primary antibodies and then the HRP-conjugated secondary antibodies (1:5000, Proteintech). The proteins were visualized by using the western blot detection kit (Advansta) and detected by chemiluminescence imaging system (ImageQuant LSA 4000 mini, GE).

Luciferase assays

HEK293T cells were seeded in a 24-well plate containing culture medium as described above. After overnight incubation, cells were transfected with the plasmids encoding PSpry, 2CARD, and Luciferase under the IFN-β promoter by using the calcium phosphate transfection method. A control reporter construct containing Renilla luciferase (Promega) was cotransfected for normalization of the transfection efficiency. At 48 h post-transfection, cells were washed with PBS and lysed with the passive lysis buffer (Promega). The culture plates were placed on a rocking platform for 15 min at room temperature. The dual luciferase activities were determined with the Promega dual-luciferase reporter kit (Promega) and GloMax20/20 single-tube luminometer (Promega) following the manufacturer's instruction (Promega). Firefly luciferase activities were normalized to Renilla luciferase reporter activities and the IFN-β fold induction of WT PSpry and 2CARD was set as 1.0. The average of three independent measurements were used with the calculation of SD.

Generation of KO cell lines in HEK293T

TRIM25$^{-/-}$ HEK 293T cells were generated by CRISPR/Cas9 technique and the sg-RNA sequence was ATGTACAGTCAGATCAACG. Briefly, sg-RNA for TRIM25 were cloned into a CRISPR/Cas9-based vector pX330 with a puromycin resistance selection marker. These vectors were transfected into HEK293T cells by Lipofectamine 2000 (Invitrogen). After selection with puromycin (0.5 mg/ml), single-colonies were picked and verified by genome sequencing and immunoblotting.

Virus titer determination

VSV was a generous gift from T. Zhang (School of Public Health, Xiamen University). HEK293T and TRIM25$^{-/-}$ cells were seeded in a 6-well plate containing culture medium as described above. After overnight incubation, cells were transfected with plasmids of a control vector, WT TRIM25, or its mutants. After 24h incubation, HEK293T and TRIM25$^{-/-}$ cells in triplicate were infected with VSV (0.00000022 pfu/cell), followed by incubation at 37 °C in 2% heat-inactivated FBS DMEM for 48 h. The virus titers were determined by plaque assay in Vero E6 cells. Vero E6 cells were infected with a gradient-diluted virus sample. After a 1.5 h incubation, the supernatant was discarded. A mixture of 10% FBS DMEM and 2% agarose medium was added to a 6-well plate and allowed to cool before incubation at 37 °C for 48 h. The cells were then fixed with 4% paraformaldehyde and stained with crystal violet for counting the number of plaques.

Quantification and statistical analysis

Crystallographic statistics were generated during refinement with Phenix and can be found in Table S1. Model was generated and analyzed with Discovery Studio. The analysis of the interacting interface in the PSpry/2CARD complex could be found in Table S3. Statistical analyses were done with Graphpad Prism (GraphPad Software). The number of replicates and statistical method for each experiment were indicated in the corresponding figures.

Data availability

All data will be available upon request. Atomic coordinates and structure factors for the crystal structure of the TRIM25 PSpry have been deposited with the Protein Data Bank with PDB code 9IUN.

Supporting information—This article contains supporting information.

Acknowledgments—We thank the generous gift of VSV from T. Zhang (School of Public Health, Xiamen University). We also thank all members of BL18U1/BL19U1 beamlines at SSRF of the National Facility for Protein Science in Shanghai (NFPS), Shanghai Advanced Research Institute, Chinese Academy of Sciences, for providing technical support in X-ray diffraction data collection and analysis.

Author contributions—Y. L. and X. T. writing–original draft; Y. L. visualization; Y. L., X. C., and T. L. validation; Y. L., W. H., D. L., H. Y., and J. H. software; Y. L., W. H., D. L., H. Y., and J. H. methodology; Y. L., S. W., X. T., C. K., W. H., T. X., S. W., Z. W., Z. S., H. R., Y. S., L. H., X. C., and T. L. investigation; Y. L., S. W., C. K., W. H., T. X., S. W., Z. W., Z. S., H. R., Y. S., L. H., X. C., and T. L. formal analysis; Y. L., X. T., and C. K. data curation; Y. L., X. T., and T. L. conceptualization; D. L., H. Y., J. H., X. C., and T. L. supervision; Y. L., X. C., and T. L. writing–review and editing; X. C. and T. L. resources; X. C. and T. L. project administration; X. C. and T. L. funding acquisition.

Funding and additional information—This study was supported by the National Natural Science Foundation of China (No. 31670729), Fujian Natural Science Foundation (2022J02057), Traditional Chinese Medicine Foundation of Xiamen (XWZY-2023-0602), as well as Xiamen Medical and Health Key Projects (3502Z20234016).

Conflicts of interest—The authors declare that they have no conflicts of interests with the contents of this article.

Abbreviations—The abbreviations used are: 2CARD, Two caspase activation and recruitment domains; CC, Coiled-coil; MAVS, Mitochondrial antiviral signaling protein; MTSL, (1-oxyl-2,2,5,5-tetramethyl-3-pyrroline-3-methyl) methane thiosulfonate; PRE, Paramagnetic relaxation enhancement; PSpry, SPRY/SPla and the

RYanodine receptor; RIG-I, Retinoic acid inducible gene-I; RING, Really interesting new gene; VSV, Vesicular stomatitis virus.

References

1. Goubau, D., Deddouche, S., and Reis e Sousa, C. (2013) Cytosolic sensing of viruses. *Immunity* **38**, 855–869
2. Schlee, M. (2013) Master sensors of pathogenic rna - rig-i like receptors. *Immunobiology* **218**, 1322–1335
3. Cui, S., Eisenacher, K., Kirchhofer, A., Brzozka, K., Lammens, A., Lammens, K., *et al.* (2008) The c-terminal regulatory domain is the rna 5'-triphosphate sensor of rig-i. *Mol. Cell* **29**, 169–179
4. Gack, M. U., Kirchhofer, A., Shin, Y. C., Inn, K. S., Liang, C., Cui, S., *et al.* (2008) Roles of rig-i n-terminal tandem card and splice variant in trim25-mediated antiviral signal transduction. *Proc. Natl. Acad. Sci. U. S. A.* **105**, 16743–16748
5. Luo, D., Ding, S. C., Vela, A., Kohlway, A., Lindenbach, B. D., and Pyle, A. M. (2011) Structural insights into rna recognition by rig-i. *Cell* **147**, 409–422
6. Kowalinski, E., Lunardi, T., McCarthy, A. A., Louber, J., Brunel, J., Grigorov, B., *et al.* (2011) Structural basis for the activation of innate immune pattern-recognition receptor rig-i by viral rna. *Cell* **147**, 423–435
7. Ferrage, F., Dutta, K., Nistal-Villan, E., Patel, J. R., Sanchez-Aparicio, M. T., De Ioannes, P., *et al.* (2012) Structure and dynamics of the second card of human rig-i provide mechanistic insights into regulation of rig-i activation. *Structure* **20**, 2048–2061
8. Jiang, X., Kinch, L. N., Brautigam, C. A., Chen, X., Du, F., Grishin, N. V., and Chen, Z. J. (2012) Ubiquitin-induced oligomerization of the rna sensors rig-i and mda5 activates antiviral innate immune response. *Immunity* **36**, 959–973
9. Loo, Y. M., and Gale, M., Jr. (2011) Immune signaling by rig-i-like receptors. *Immunity* **34**, 680–692
10. Xu, H., He, X., Zheng, H., Huang, L. J., Hou, F., Yu, Z., *et al.* (2014) Structural basis for the prion-like mavs filaments in antiviral innate immunity. *Elife* **3**, e01489
11. van Gent, M., Sparrer, K. M. J., and Gack, M. U. (2018) Trim proteins and their roles in antiviral host defenses. *Annu. Rev. Virol.* **5**, 385–405
12. Versteeg, G. A., Rajsbaum, R., Sanchez-Aparicio, M. T., Maestre, A. M., Valdiviezo, J., Shi, M., *et al.* (2013) The e3-ligase trim family of proteins regulates signaling pathways triggered by innate immune pattern-recognition receptors. *Immunity* **38**, 384–398
13. Zeng, W., Sun, L., Jiang, X., Chen, X., Hou, F., Adhikari, A., *et al.* (2010) Reconstitution of the rig-i pathway reveals a signaling role of unanchored polyubiquitin chains in innate immunity. *Cell* **141**, 315–330
14. Gack, M. U., Shin, Y. C., Joo, C. H., Urano, T., Liang, C., Sun, L., *et al.* (2007) Trim25 ring-finger e3 ubiquitin ligase is essential for rig-i-mediated antiviral activity. *Nature* **446**, 916–920
15. D'Cruz, A. A., Kershaw, N. J., Chiang, J. J., Wang, M. K., Nicola, N. A., Babon, J. J., *et al.* (2013) Crystal structure of the trim25 b30.2 (pryspry) domain: A key component of antiviral signalling. *Biochem. J.* **456**, 231–240
16. Koliopoulos, M. G., Esposito, D., Christodoulou, E., Taylor, I. A., and Rittinger, K. (2016) Functional role of trim e3 ligase oligomerization and regulation of catalytic activity. *EMBO J.* **35**, 1204–1218
17. Berndsen, C. E., and Wolberger, C. (2014) New insights into ubiquitin e3 ligase mechanism. *Nat. Struct. Mol. Biol.* **21**, 301–307
18. Meroni, G., and Diez-Roux, G. (2005) Trim/rbcc, a novel class of 'single protein ring finger' e3 ubiquitin ligases. *Bioessays* **27**, 1147–1157
19. Yudina, Z., Roa, A., Johnson, R., Biris, N., de Souza Aranha Vieira, D. A., Tsiperson, V., *et al.* (2015) Ring dimerization links higher-order assembly of trim5alpha to synthesis of k63-linked polyubiquitin. *Cell Rep.* **12**, 788–797
20. Dou, H., Buetow, L., Sibbet, G. J., Cameron, K., and Huang, D. T. (2012) Birc7-e2 ubiquitin conjugate structure reveals the mechanism of ubiquitin transfer by a ring dimer. *Nat. Struct. Mol. Biol.* **19**, 876–883
21. Sanchez, J. G., Okreglicka, K., Chandrasekaran, V., Welker, J. M., Sundquist, W. I., and Pornillos, O. (2014) The tripartite motif coiled-coil is an elongated antiparallel hairpin dimer. *Proc. Natl. Acad. Sci. U. S. A.* **111**, 2494–2499
22. Hayman, T. J., Hsu, A. C., Kolesnik, T. B., Dagley, L. F., Willemsen, J., Tate, M. D., *et al.* (2019) Riplet, and not trim25, is required for endogenous rig-i-dependent antiviral responses. *Immunol. Cell Biol.* **97**, 840–852
23. Choudhury, N. R., Trus, I., Heikel, G., Wolczyk, M., Szymanski, J., Bolembach, A., *et al.* (2022) Trim25 inhibits influenza a virus infection, destabilizes viral mrna, but is redundant for activating the rig-i pathway. *Nucleic Acids Res.* **50**, 7097–7114
24. Cadena, C., Ahmad, S., Xavier, A., Willemsen, J., Park, S., Park, J. W., *et al.* (2019) Ubiquitin-dependent and -independent roles of e3 ligase riplet in innate immunity. *Cell* **177**, 1187–1200.e1116
25. Zhao, Y., Sui, L., Wu, P., Wang, W., Wang, Z., Yu, Y., *et al.* (2021) A dual-role of sars-cov-2 nucleocapsid protein in regulating innate immune response. *Signal Transduct. Target Ther.* **6**, 331
26. Yang, Z., Li, J., Li, J., Zheng, H., Li, H., Lai, Q., *et al.* (2022) Engagement of the g3bp2-trim25 interaction by nucleocapsid protein suppresses the type i interferon response in sars-cov-2-infected cells. *Vaccines (Basel)* **10**, 2042
27. Ohta, K., Saka, N., and Nishio, M. (2022) Hazara orthonairovirus nucleoprotein antagonizes type i interferon production by inhibition of rig-i ubiquitination. *Viruses* **14**, 1965
28. Hu, Q. X., Wang, H. Y., Jiang, L., Wang, C. Y., Ju, L. G., Zhu, Y., *et al.* (2021) Histone demethylase lsd1 promotes rig-i poly-ubiquitination and anti-viral gene expression. *PLoS Pathog.* **17**, e1009918
29. Jiang, J., Li, Y., Sun, Z., Gong, L., Li, X., Shi, F., *et al.* (2022) Lncnspl facilitates influenza a viral immune escape by restricting trim25-mediated k63-linked rig-i ubiquitination. *iScience* **25**, 104607
30. Gori Savellini, G., Anichini, G., Gandolfo, C., and Cusi, M. G. (2021) Sars-cov-2 n protein targets trim25-mediated rig-i activation to suppress innate immunity. *Viruses* **13**, 1439
31. Oh, S. J., and Shin, O. S. (2021) Sars-cov-2 nucleocapsid protein targets rig-i-like receptor pathways to inhibit the induction of interferon response. *Cells* **10**, 530
32. Chiang, C., Dvorkin, S., Chiang, J. J., Potter, R. B., and Gack, M. U. (2021) The small t antigen of jc virus antagonizes rig-i-mediated innate immunity by inhibiting trim25's rna binding ability. *mBio* **12**, e00620
33. van Gent, M., Chiang, J. J., Muppala, S., Chiang, C., Azab, W., Kattenhorn, L., *et al.* (2022) The us3 kinase of herpes simplex virus phosphorylates the rna sensor rig-i to suppress innate immunity. *J Virol* **96**, e0151021
34. Zhang, B., Cai, T., He, H., Huang, X., Luo, Y., Huang, S., *et al.* (2023) Trim25 suppresses rabies virus fixed hep-flury strain production by activating rig-1-mediated type i interferons. *Genes (Basel)* **14**, 1555
35. Song, H., Xiao, Q., Xu, F., Wei, Q., Wang, F., and Tan, G. (2023) Trim25 inhibits hbv replication by promoting hbx degradation and the rig-i-mediated pgrna recognition. *Chin. Med. J.* **136**, 799–806
36. Yuan, Y., Fang, A., Wang, Z., Tian, B., Zhang, Y., Sui, B., *et al.* (2022) Trim25 restricts rabies virus replication by destabilizing phosphoprotein. *Cell. Insight* **1**, 100057
37. Okamoto, M., Kouwaki, T., Fukushima, Y., and Oshiumi, H. (2017) Regulation of rig-i activation by k63-linked polyubiquitination. *Front. Immunol.* **8**, 1942
38. Syafrizayanti, Betzen, C., Hoheisel, J. D., and Kastelic, D. (2014) Methods for analyzing and quantifying protein-protein interaction. *Expert Rev. Proteomics* **11**, 107–120
39. Kong, C., Penumutchu, S. R., Hung, K. W., Huang, H., Lin, T., and Yu, C. (2015) Backbone resonance assignments of the pryspry domain of trim25. *Biomol NMR Assign* **9**, 313–315
40. Dominguez, C., Boelens, R., and Bonvin, A. M. (2003) Haddock: A protein-protein docking approach based on biochemical or biophysical information. *J. Am. Chem. Soc.* **125**, 1731–1737
41. Kato, K., Ahmad, S., Zhu, Z., Young, J. M., Mu, X., Park, S., *et al.* (2021) Structural analysis of rig-i-like receptors reveals ancient rules of engagement between diverse rna helicases and trim ubiquitin ligases. *Mol. Cell* **81**, 599–613.e598
42. Mao, B., Tejero, R., Baker, D., and Montelione, G. T. (2014) Protein nmr structures refined with rosetta have higher accuracy relative to corresponding x-ray crystal structures. *J. Am. Chem. Soc.* **136**, 1893–1906

43. Card, P. B., Erbel, P. J., and Gardner, K. H. (2005) Structural basis of arnt pas-b dimerization: Use of a common beta-sheet interface for hetero- and homodimerization. *J. Mol. Biol.* **353**, 664–677
44. Clore, G. M., Tang, C., and Iwahara, J. (2007) Elucidating transient macromolecular interactions using paramagnetic relaxation enhancement. *Curr. Opin. Struct. Biol.* **17**, 603–616
45. Koliopoulos, M. G., Lethier, M., van der Veen, A. G., Haubrich, K., Hennig, J., Kowalinski, E., *et al.* (2018) Molecular mechanism of influenza a ns1-mediated trim25 recognition and inhibition. *Nat. Commun.* **9**, 1820
46. Sanchez, J. G., Sparrer, K. M. J., Chiang, C., Reis, R. A., Chiang, J. J., Zurenski, M. A., *et al.* (2018) Trim25 binds rna to modulate cellular antiviral defense. *J. Mol. Biol.* **430**, 5280–5293
47. Peisley, A., Wu, B., Xu, H., Chen, Z. J., and Hur, S. (2014) Structural basis for ubiquitin-mediated antiviral signal activation by rig-i. *Nature* **509**, 110–114
48. Winn, M. D., Ballard, C. C., Cowtan, K. D., Dodson, E. J., Emsley, P., Evans, P. R., *et al.* (2011) Overview of the ccp4 suite and current developments. *Acta Crystallogr. D Biol. Crystallogr.* **67**, 235–242
49. Liebschner, D., Afonine, P. V., Baker, M. L., Bunkoczi, G., Chen, V. B., Croll, T. I., *et al.* (2019) Macromolecular structure determination using x-rays, neutrons and electrons: recent developments in phenix. *Acta Crystallogr. D Biol. Crystallogr.* **75**, 861–877
50. Emsley, P., and Cowtan, K. (2004) Coot: Model-building tools for molecular graphics. *Acta Crystallogr. D Biol. Crystallogr.* **60**, 2126–2132
51. Farmer, B. T., 2nd, Constantine, K. L., Goldfarb, V., Friedrichs, M. S., Wittekind, M., Yanchunas, J., Jr., *et al.* (1996) Localizing the nadp+ binding site on the murb enzyme by nmr. *Nat. Struct. Biol.* **3**, 995–997